A Combined Fit of the Diffuse Neutrino Spectrum using IceCube Muon Tracks and Cascades

The IceCube Collaboration

(a complete list of authors can be found at the end of the proceedings)
E-mail: erik.ganster@icecube.wisc.edu, rnaab@icecube.wisc.edu,
zelong.zhang@icecube.wisc.edu

The IceCube Neutrino Observatory first observed a diffuse flux of high energy astrophysical neutrinos in 2013. Since then, this observation has been confirmed in multiple detection channels such as high energy starting events, cascades, and through-going muon tracks. Combining these event selections into a high statistics global fit of 10 years of IceCube's neutrino data could strongly improve the understanding of the diffuse astrophysical neutrino flux: challenging or confirming the simple unbroken power-law flux model as well as the astrophysical neutrino flux composition. One key component of such a combined analysis is the consistent modelling of systematic uncertainties of different event selections. This can be achieved using the novel SnowStorm Monte Carlo method which allows constraints to be placed on multiple systematic parameters from a single simulation set. We will report on the status of a new combined analysis of through-going muon tracks and cascades. It is based on a consistent all flavor neutrino signal and background simulation using, for the first time, the SnowStorm method to analyze IceCube's high-energy neutrino data. Estimated sensitivities for the energy spectrum of the diffuse astrophysical neutrino flux will be shown.

Corresponding authors: Erik Ganster[1][*], Richard Naab [2], Zelong Zhang[3]

[1] *RWTH Aachen University*

[2] *DESY Zeuthen*

[3] *Stony Brook University*

[*] Presenter

1. Introduction

Since the discovery of a high energy astrophysical neutrino flux in 2013 [1], the IceCube Neutrino Observatory has confirmed the measurement of a diffuse extra-galactic neutrino flux in several detection channels such as: high energy starting events [2], through-going muon tracks [3] and cascades [4]. The measurements prefer a single power-law (SPL) energy spectrum for the astrophysical neutrino flux, and the measured properties (normalization and spectral index) by these complementary analyses are consistent within uncertainties.

In 2015, the first combined analysis of IceCube's high energy neutrino data was performed [5]. A new combined analysis targeting the energy spectrum of the diffuse astrophysical neutrino flux and utilizing the higher statistics of the complementary track-like and cascade detection channels in IceCube is currently being prepared. Here, we report on the current status and estimated sensitivity of this combined analysis. It relies on consistent modeling of the neutrino flux components and corresponding uncertainties as well as a consistent treatment of detector systematic uncertainties across all measurement channels. We use a novel Monte Carlo (MC) simulation technique and present a new method for including this MC in an analysis.

2. A novel approach for including detector systematic uncertainties

A combination of multiple event selections into a combined fit relies on consistent modeling of not only the signal parameters but also the systematic uncertainties. The analysis presented here is based on the SnowStorm method [6] for treating systematic uncertainties within each individual event selection (cascades and through-going tracks).

The central element of the SnowStorm simulation method (as presented in [6]) is the so-called "SnowStorm event ensemble": each event[1] is simulated with a set of certain nuisance parameter values that are continuously sampled from a distribution defined in advance. The result of this is an ensemble of events, each representing a different combination of nuisance parameters in the pre-defined nuisance parameter phase-space.

The method presented here will re-weight the simulated distribution of events according to the current choice of nuisance parameter values in the fit. This is different from using the event ensemble to obtain the gradient of the analysis observables with respect to the nuisance parameters shown in [6]. To obtain the event distribution in the analysis space for a discrete choice of some nuisance parameter η, the SnowStorm event ensemble is re-weighted to a Gaussian distribution in η: $p_{\text{sys}}(\eta) = \mathcal{G}(\eta, \mu, \sigma)$. The mean value μ is set to the value of η that one wants to obtain a prediction for, while σ can be used to limit the range used for re-weighting. The per-event re-weighting factor w is then given by:

$$w(\eta) = \frac{p_{\text{sys}}(\eta)}{p_{\text{sys}}^{\text{sim}}(\eta)},$$

where the denominator takes the finite phase space of the sampling distribution $p_{\text{sys}}^{\text{sim}}(\eta)$ used during simulation into account. Assuming the effect of the systematic uncertainties to be sufficiently small so that variations can be treated perturbatively (neglecting $O(\eta^2)$ terms) as in [6], the re-weighted

---

[1]For computational reasons a few events are grouped and treated the same.
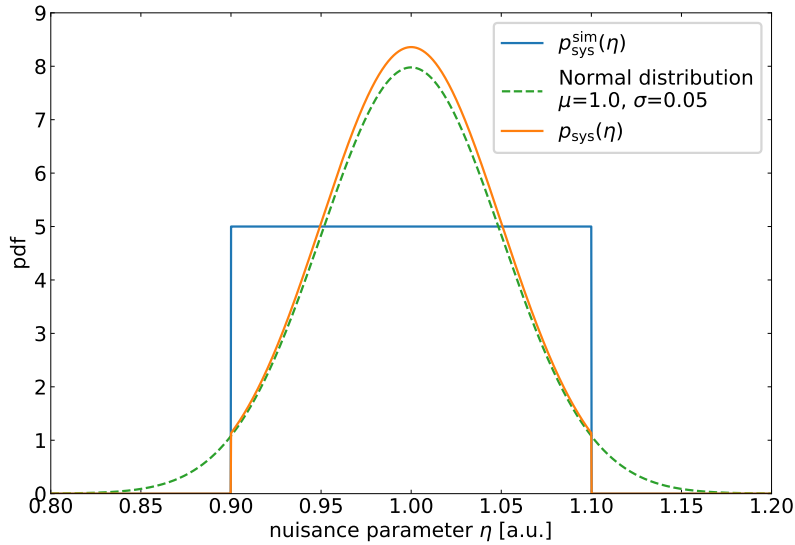
Figure 1: Sketch of re-weighting a SnowStorm event ensemble. The uniformly sampled nuisance parameter η (blue), but is re-weighted to a Gaussian/normal distribution for use in the analysis (orange). To account for the simulated phase space, in this case $0.9 < \eta < 1.1$, during simulation, the Gaussian distribution (green) needs to be re-normalized to represent a proper probability density function (orange).

event ensemble will yield the event distribution for a discrete choice of $\eta = \mu$. This re-weighting can be applied for multiple nuisance parameters at the same time by expanding the above calculation to all nuisance parameters $\vec{\eta} = (\eta_0, \eta_1, \ldots, \eta_i)$ for which a re-weighting should be applied:

$$w(\vec{\eta}) = \prod_i \frac{p_{\text{sys}}(\eta_i)}{p_{\text{sys}}^{\text{sim}}(\eta_i)} \ .$$

This concept of re-weighting is not limited to a Gaussian re-weighting distribution. Any symmetric $p_{sys}(\eta_i)$ distribution will yield to the prediction of $\eta_i = \langle p_{sys}(\eta_i) \rangle$. Figure 1 shows the relative contribution to the final analysis event distribution as a function of the nuisance parameter value η for the case of $p_{sys} = \mathcal{G}(\eta, \mu, \sigma)$. For a Gaussian, weights events with a value of η close to μ have a higher weighting factor than events further away.

We have successfully used a SnowStorm neutrino event ensemble with this re-weighting method to take the same systematic uncertainties as used in the individual analyses in [3] and [4] (optical efficiency, bulk ice absorption and scattering, and hole ice) into account. Comparisons of this SnowStorm re-weighting treatment with the systematics treatment previously used in the individual analyses showed very similar results.

3. Monte Carlo Event Samples and Analysis method

3.1 The Event Samples

This work aims to combine two of IceCube's neutrino data samples, through-going muon tracks and cascades, into a single analysis. Individual analyses have been performed on both event samples, confirming the observation of a high energy astrophysical neutrino flux [3, 4].

3

The through-going muon track sample used in [3] and [7] focuses on up-going track-like events with a reconstructed zenith angle $\theta_{\mathrm{reco}} > 85°$. This cut uses the Earth as a shield against the background of atmospheric muons reaching the IceCube in-ice neutrino detector. This background is further reduced by a boosted decision tree (BDT) trained to separate atmospheric muons from muons originating from charged current muon-neutrino interactions. The result is a high purity (99.7 %) sample of muon neutrinos of either atmospheric or astrophysical origin [3].

The cascade data sample used in [4] is a full-sky sample and consists of three sub-samples, cascade signal sample, muon control sample and hybrid sample [8]. It selects on low level cascade events in low and high energy regimes and is classified into three sub-samples by the low energy event selection. The low energy event selection mainly uses a BDT method [8] but the high energy ($E_{\mathrm{reco}} > 60\,\mathrm{TeV}$) event selection uses straight cuts [9]. The cascade signal sample is dominated by conventional atmospheric neutrinos and astrophysical neutrinos. The muon background only contributes $\sim 8\%$ to it [8]. The events are binned into 3 zenith bins, corresponding to northern, horizontal and southern sky and 22 energy bins from $10^{2.6}$ to 10^7 GeV [8]. Since the astrophysical neutrino spectrum fitted in single power law is harder than atmospheric neutrino spectrum, this sample is dominated by atmospheric neutrinos at low energy but astrophysical neutrinos at high energy. The muon control sample is not binned. It is dominated by atmospheric muons ($\sim 65\%$) and it is used to constrain the normalization of atmospheric muon part in cascade analysis [8]. The hybrid sample is binned into 11 energy bins. It is dominated by conventional atmospheric muon neutrinos interacting via the charged current channel, so it is used to constrain the atmospheric neutrino part in original cascade analysis [8].

3.2 Analysis Method

Both individual analyses use a two dimensional Likelihood fit of reconstructed energy and zenith (E_{reco} and $\cos(\theta_{\mathrm{reco}})$) for analyzing the data. In the case of fully disjunct samples, a combined Likelihood can be obtained by building the product of the, in this case independent, per-bin Likelihoods:

$$\mathcal{L}_{\mathrm{combined}} = \prod_{\mathrm{bin}\,i}^{N_{\mathrm{bins}}} \mathcal{L}_i\left(n_i, \mu_i(\vec{\rho}, \vec{\eta})\right) \times \prod_j \pi(\eta_j),$$

where the number of events n_i in analysis histogram bin i is compared to the expected number of events μ_i using a Poisson likelihood $\mathcal{L}_i$. The expectation μ_i is a function of the signal ($\vec{\rho}$) and nuisance ($\vec{\eta}$) parameters. Priors $\pi(\eta_j)$ on the nuisance parameters η_j are chosen as described in Table 1.

This is only valid if both individual analysis histograms have no common² events. Despite focusing on two different event topologies in the detector, there is some overlap between IceCube's through-going track and cascade event selection. For the Cascade signal and muon sample, there is only a marginal overlap (0.1 %) with the tracks sample. This can easily be eliminated by assigning a tag to those overlapping events and using them only once when constructing the analysis histograms.

However, as the hybrid sub-selection of the cascade sample is optimized for starting events with a track-like signature in the detector, about 30 % of these events also pass the through-going

---

²and thus "overlapping"

Name		Allowed Range	Prior
spectral index	γ_{astro}	$[1.0, \infty)$	-
flux normalization	Φ_0^{astro}	$[0.0, \infty)$	-
Conventional Flux Normalization		$[0.0, \infty)$	-
Prompt Flux Normalization		$[0.0, \infty)$	-
Muon Flux Normalization (cascades only)		$[0.0, \infty)$	-
Cosmic-Ray model interpolation	λ_{CRModel}	$[-1.0, +2.0]$	$\mathcal{G}(0.0, 1.0)$
Cosmic-Ray spectral index shift	$\Delta_{\gamma_{\text{CR}}}$	$[-1.0, +1.0]$	-
Optical Efficiency		$[0.9, 1.1]$	-
Bulk Ice Absorption		$[0.9, 1.1]$	-
Bulk Ice Scattering		$[0.9, 1.1]$	-
Hole-Ice p_0		$[-1.0, +1.0]$	-

Table 1: All used fit parameters, their allowed ranges, and Gaussian priors $\mathcal{G}(\mu, \sigma)$ (if used). The horizontal lines separate the signal parameters from the flux and detector nuisance parameters (from top to bottom).

track selection. In the individual analysis of IceCube's cascade data, the starting track sub-sample is used to constrain the normalization of the atmospheric neutrino flux [8]. In the combined fit presented here, the large statistics of the tracks sample allows an even tighter constraint of the atmospheric neutrino flux normalization. Therefore, we do not include the cascade hybrid selection in this combined analysis. We fit the tracks sample as well as the cascade signal and cascade muon control sample.

3.3 Fit parameters

We model the astrophysical neutrino component with a SPL in the form:

$$\Phi_{\nu+\bar{\nu}}^{\text{astro}} = c_{\text{units}} \times \Phi_0^{\text{astro}} \times \left(\frac{E_\nu}{100\,\text{TeV}} \right)^{-\gamma_{\text{astro}}} , \tag{1}$$

with the flux normalization Φ_0^{astro} and the spectral index γ_{astro} as two free parameters in units of $c_{\text{units}} = 10^{-18}\,\text{GeV}^{-1}\,\text{cm}^{-2}\,\text{s}^{-1}\,\text{sr}^{-1}$. We further assume an equal flux of all neutrino flavors as well as neutrinos and antineutrinos. The shape of the spectrum of both conventional and prompt atmospheric neutrino fluxes is obtained using the Matrix-CascadeEquation solver package MCEq [10], and the normalizations of both are left floating. We allow for slight spectral distortions of the primary cosmic ray model, as well as an interpolation between the two primary cosmic ray models H4a and GST4 (as in the previous iteration of the tracks analysis [7]). An independent normalization of the flux of atmospheric muons contributing to the cascade event sample is also left floating in the fit.

Finally, the likelihood also depends on some detector systematic parameters, which are treated using the re-weighting method of the used SnowStorm event ensemble as explained in 2. In agreement with the latest standalone analyses, we include variations in the optical efficiency, the absorption and scattering coefficients of the bulk ice as well as variations in the parameter controlling

for effects of the refrozen hole-ice [4, 7]. Using the re-weighting method presented here, we obtain very similar results compared to the systematic treatment previously used in the individual analyses.

4. Results/Sensitivities

Table 2 lists the estimated sensitivities of the combined fit. For the Asimov signal, the best fit of [7] was assumed. We further assumed a lifetime of 10 years for all fits. The estimated 68% CL contours for the astrophysical signal parameters are shown in Figure 2. The sensitivities for the individual through-going track and cascade analysis, assuming the same Asimov signal and lifetime, are shown for comparison. Compared to these, the sensitivity of the combined analysis of both event selections is strongly increased.

	through-going tracks	cascades	combined fit
flux normalization Φ_0^{astro}	$1.36^{+0.21}_{-0.65}$	$1.36^{+0.11}_{-0.17}$	$1.36^{+0.09}_{-0.15}$
spectral index γ_{astro}	$2.37^{+0.08}_{-0.23}$	$2.37^{+0.05}_{-0.07}$	$2.37^{+0.04}_{-0.05}$

Table 2: Estimated 68% sensitivities for an Asimov signal fit of an injected single power-law astrophysical neutrino flux.

The smaller size of the contours for cascades compared to the tracks results from the much better energy resolution of shower-type events (mainly selected by cascade selection) compared to track events: Whereas in the case of cascades, a "calorimetric" measurement of the energy is possible, the measurement of the energy of a muon only provides a lower limit to the parent neutrino's energy when the muon was produced outside the detector. On the other hand, the large effective area of the track selection leads to a much higher rate of observed events which constrains the nuisance parameters of the atmospheric fluxes and detector systematic uncertainties much more as in an analysis targeting cascades only.

As explained in Section 3.2, a decision has to be made about the overlapping events: They can be used either in the tracks sample or in the cascade sample(s). What we find is that the measurement of the astrophysical signal parameters is independent of the decision made. Given the small number of overlapping events in total as well as the fact that starting tracks do not constitute the actual signal for the cascade sample, this is not surprising.

Figure 3 shows the spectrum inferred from the combined fit, along with the result of fitting a piecewise model to the assumed signal. The piecewise model assumes independent normalizations in each segment of neutrino energy, with a fixed spectral index of $\gamma_{\text{astro}} = -2$ in every energy bin. The flux level of atmospheric neutrinos is shown for comparison. In our combined analysis, the flux is determined most precisely around 100 TeV. At higher energies, where atmospheric backgrounds are low, we expect a low number of events overall, which limits the analysis. At lower energies, the astrophysical flux is subdominant, limiting the precision to which it can be measured. In the case of down-going events, atmospheric neutrinos can be accompanied by muons produced in the same air shower. These muons are vetoed in the cascade event selection so that atmospheric neutrinos have a certain "self-veto" probability to be discarded by the selection criteria. The suppression factor can be $\gtrsim 10$ for very down-going neutrinos at 10 TeV [8], so that the sensitivity to the astrophysical flux in the corresponding zenith analysis bins extends to lower energies.
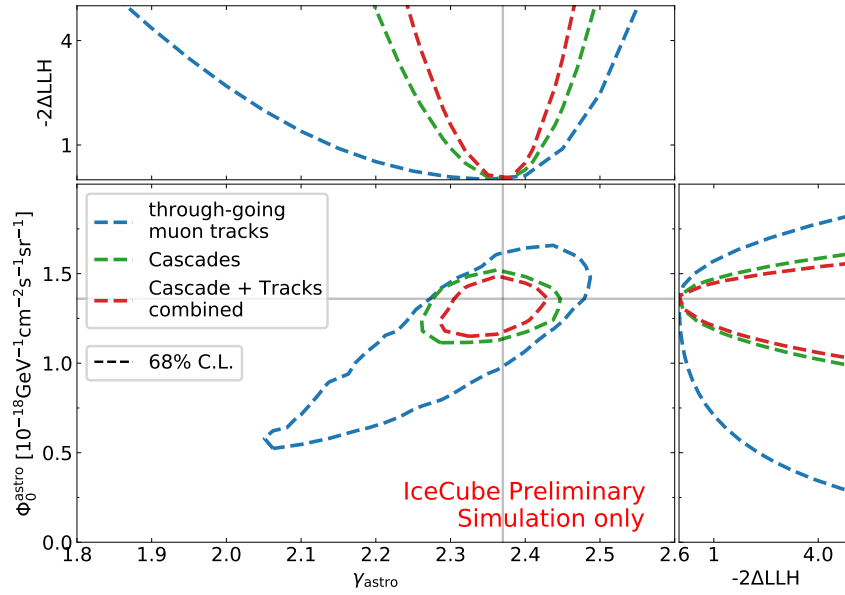
Figure 2: 68% CL contours of the signal parameters Φ_0^{astro} and γ_{astro}. The red line shows the fit of combining track and cascade (Asimov) data, individual fit results are shown in blue (tracks) and green (cascades). For all contours, a single power-law flux was used for generating the Asimov signal and in the hypothesis used for fitting. Grey lines show the parameter values of the generated Asimov signal. The top and right plots show 1D profile Likelihood scans of both signal parameters.

5. Conclusions and Outlook

We have presented the current status of a combined diffuse fit of IceCube's high energy cascade and through-going muon track neutrino data. This study makes use of a SnowStorm MC event ensemble and a new method for analyzing this ensemble as described in Section 2. This provides a consistent treatment of the detector systematic nuisance parameters for both event selections. Along with using MCEq for obtaining the atmospheric neutrino contributions, this allows for a combination of the cascade and through-going muon track event selections into a single Likelihood analysis.

The sensitivities presented in Section 4 assume a livetime of 10 years and will allow to challenge the so far single-power law modeled astrophysical neutrino flux. The benefits of combining different analyses were demonstrated by comparing our result to the individual analyses using exactly the same modeling. The approach presented here can be easily extended to included further detection channels as well as additional uncertainties on the atmospheric fluxes or the modeling of the ice. This will be investigated further in the future.

References

[1] **IceCube** Collaboration, M. G. Aartsen *et al. Science* **342** (2013) 1242856.

[2] **IceCube** Collaboration, R. Abbasi *et al. Phys. Rev. D* **104** (Jul, 2021) 022002.

[3] **IceCube** Collaboration, M. G. Aartsen *et al. Astrophys. J.* **833** no. 1, (2016) 3.
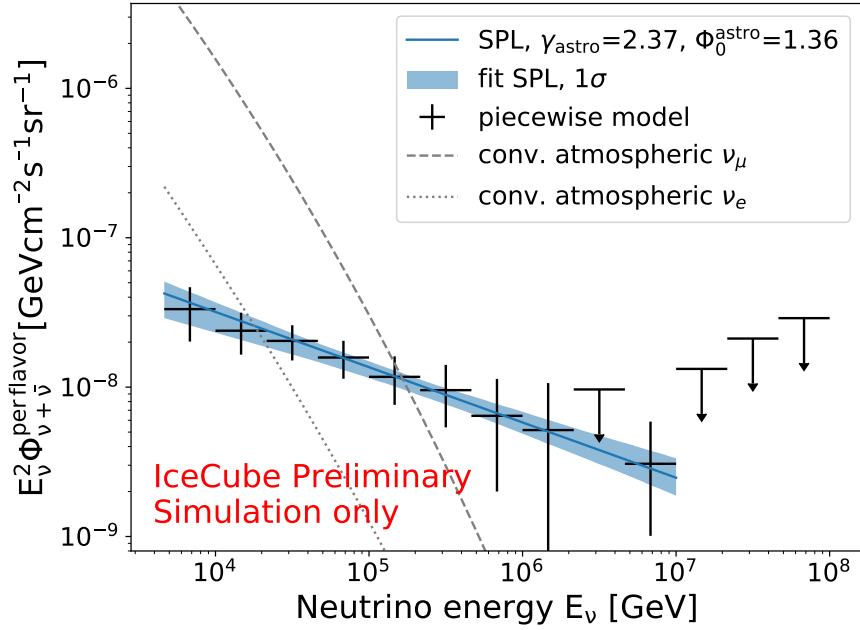
Figure 3: Inferred neutrino spectrum from the combined analysis. The blue line represents the SPL model assumed for the study presented here. The blue region shows the estimated 1σ CL when fitting a SPL model. Alternatively, a piecewise model describing the flux with independent contributions from different bins in energy with a per-bin spectral index of -2, is fit and the results are shown in black crosses. In the highest energy segment without an upper limit, the sensitivity to astrophysical neutrinos is enhanced due to the Glashow resonance [11].

[4] **IceCube** Collaboration, M. G. Aartsen *et al. Phys. Rev. Lett.* **125** no. 12, (2020) 121104.

[5] **IceCube** Collaboration, M. G. Aartsen *et al. Astrophys. J.* **809** no. 1, (2015) 98.

[6] **IceCube** Collaboration, M. G. Aartsen *et al. JCAP* **10** (2019) 048.

[7] **IceCube** Collaboration, J. Stettner *PoS* **ICRC2019** (2020) 1017.

[8] H. Niederhausen, *Measurement of the High Energy Astrophysical Neutrino Flux Using Electron and Tau Neutrinos Observed in Four Years of IceCube Data.* PhD thesis, Stony Brook University, 2018. ISBN 978-0-438-37019-7.

[9] X. Yiqian, *Measurement of the High Energy Neutrino Interaction Cross Section Using Neutrino-Induced Electromagnetic and Hadronic Showers Observed in Five Years of IceCube Data.* PhD thesis, Stony Brook University, 2019. ISBN 978-1-687-98329-9.

[10] A. Fedynitch *et al. EPJ Web of Conferences* **99** (2015) 08001.

[11] **IceCube** Collaboration, M. G. Aartsen *et al. Nature* **591** no. 7849, (2021) 220–224. [Erratum: Nature 592, E11 (2021)].

Full Author List: IceCube Collaboration

R. Abbasi[17], M. Ackermann[59], J. Adams[18], J. A. Aguilar[12], M. Ahlers[22], M. Ahrens[50], C. Alispach[28], A. A. Alves Jr.[31], N. M. Amin[42], R. An[14], K. Andeen[40], T. Anderson[56], G. Anton[26], C. Argüelles[14], Y. Ashida[38], S. Axani[15], X. Bai[46], A. Balagopal V.[38], A. Barbano[28], S. W. Barwick[30], B. Bastian[59], V. Basu[38], S. Baur[12], R. Bay[8], J. J. Beatty[20, 21], K.-H. Becker[58], J. Becker Tjus[11], C. Bellenghi[27], S. BenZvi[48], D. Berley[19], E. Bernardini[59, 60], D. Z. Besson[34, 61], G. Binder[8, 9], D. Bindig[58], E. Blaufuss[19], S. Blot[59], M. Boddenberg[1], F. Bontempo[31], J. Borowka[1], S. Böser[39], O. Botner[57], J. Böttcher[1], E. Bourbeau[22], F. Bradascio[59], J. Braun[38], S. Bron[28], J. Brostean-Kaiser[59], S. Browne[32], A. Burgman[57], R. T. Burley[2], R. S. Busse[41], M. A. Campana[45], E. G. Carnie-Bronca[2], C. Chen[6], D. Chirkin[38], K. Choi[52], B. A. Clark[24], K. Clark[33], L. Classen[41], A. Coleman[42], G. H. Collin[15], J. M. Conrad[15], P. Coppin[13], P. Correa[13], D. F. Cowen[55, 56], R. Cross[48], C. Dappen[1], P. Dave[6], C. De Clercq[13], J. J. DeLaunay[56], H. Dembinski[42], K. Deoskar[50], S. De Ridder[29], A. Desai[38], P. Desiati[38], K. D. de Vries[13], G. de Wasseige[13], M. de With[10], T. DeYoung[24], S. Dharani[1], A. Diaz[15], J. C. Díaz-Vélez[38], M. Dittmer[41], H. Dujmovic[31], M. Dunkman[56], M. A. DuVernois[38], E. Dvorak[46], T. Ehrhardt[39], P. Eller[27], R. Engel[31, 32], H. Erpenbeck[1], J. Evans[19], P. A. Evenson[42], K. L. Fan[19], A. R. Fazely[7], S. Fiedlschuster[26], A. T. Fienberg[56], K. Filimonov[8], C. Finley[50], L. Fischer[59], D. Fox[55], A. Franckowiak[11, 59], E. Friedman[19], A. Fritz[39], P. Fürst[1], T. K. Gaisser[42], J. Gallagher[37], E. Ganster[1], A. Garcia[14], S. Garrappa[59], L. Gerhardt[9], A. Ghadimi[54], C. Glaser[57], T. Glauch[27], T. Glüsenkamp[26], A. Goldschmidt[9], J. G. Gonzalez[42], S. Goswami[54], D. Grant[24], T. Grégoire[56], S. Griswold[48], M. Gündüz[11], C. Günther[1], C. Haack[27], A. Hallgren[57], R. Halliday[24], L. Halve[1], F. Halzen[38], M. Ha Minh[27], K. Hanson[38], J. Hardin[38], A. A. Harnisch[24], A. Haungs[31], S. Hauser[1], D. Hebecker[10], K. Helbing[58], F. Henningsen[27], E. C. Hettinger[24], S. Hickford[58], J. Hignight[25], C. Hill[16], G. C. Hill[2], K. D. Hoffman[19], R. Hoffmann[58], T. Hoinka[23], B. Hokanson-Fasig[38], K. Hoshina[38, 62], F. Huang[56], M. Huber[27], T. Huber[31], K. Hultqvist[50], M. Hünnefeld[23], R. Hussain[38], S. In[52], N. Iovine[12], A. Ishihara[16], M. Jansson[50], G. S. Japaridze[5], M. Jeong[52], B. J. P. Jones[4], D. Kang[31], W. Kang[52], X. Kang[45], A. Kappes[41], D. Kappesser[39], T. Karg[59], M. Karl[27], A. Karle[38], U. Katz[26], M. Kauer[38], M. Kellermann[1], J. L. Kelley[38], A. Kheirandish[56], K. Kin[16], T. Kintscher[59], J. Kiryluk[51], S. R. Klein[8, 9], R. Koirala[42], H. Kolanoski[10], T. Kontrimas[27], L. Köpke[39], C. Kopper[24], S. Kopper[54], D. J. Koskinen[22], P. Koundal[31], M. Kovacevich[45], M. Kowalski[10, 59], T. Kozynets[22], E. Kun[11], N. Kurahashi[45], N. Lad[59], C. Lagunas Gualda[59], J. L. Lanfranchi[56], M. J. Larson[19], F. Lauber[58], J. P. Lazar[14, 38], J. W. Lee[52], K. Leonard[38], A. Leszczyńska[32], Y. Li[56], M. Lincetto[11], Q. R. Liu[38], M. Liubarska[25], E. Lohfink[39], C. J. Lozano Mariscal[41], L. Lu[38], F. Lucarelli[28], A. Ludwig[24, 35], W. Luszczak[38], Y. Lyu[8, 9], W. Y. Ma[59], J. Madsen[38], K. B. M. Mahn[24], Y. Makino[38], S. Mancina[38], I. C. Mariş[12], R. Maruyama[43], K. Mase[16], T. McElroy[25], F. McNally[36], J. V. Mead[22], K. Meagher[38], A. Medina[21], M. Meier[16], S. Meighen-Berger[27], J. Micallef[24], D. Mockler[12], T. Montaruli[28], R. W. Moore[25], R. Morse[38], M. Moulai[15], R. Naab[59], R. Nagai[16], U. Naumann[58], J. Necker[59], L. V. Nguyễn[24], H. Niederhausen[27], M. U. Nisa[24], S. C. Nowicki[24], D. R. Nygren[9], A. Obertacke Pollmann[58], M. Oehler[31], A. Olivas[19], E. O'Sullivan[57], H. Pandya[42], D. V. Pankova[56], N. Park[33], G. K. Parker[4], E. N. Paudel[42], L. Paul[40], C. Pérez de los Heros[57], L. Peters[1], J. Peterson[38], S. Philippen[1], D. Pieloth[23], S. Pieper[58], M. Pittermann[32], A. Pizzuto[38], M. Plum[40], Y. Popovych[39], A. Porcelli[29], M. Prado Rodriguez[38], P. B. Price[8], B. Pries[24], G. T. Przybylski[9], C. Raab[12], A. Raissi[18], M. Rameez[22], K. Rawlins[3], I. C. Rea[27], A. Rehman[42], P. Reichherzer[11], R. Reimann[1], G. Renzi[12], E. Resconi[27], S. Reusch[59], W. Rhode[23], M. Richman[45], B. Riedel[38], E. J. Roberts[2], S. Robertson[8, 9], G. Roellinghoff[52], M. Rongen[39], C. Rott[49, 52], T. Ruhe[23], D. Ryckbosch[29], D. Rysewyk Cantu[24], I. Safa[14, 38], J. Saffer[32], S. E. Sanchez Herrera[24], A. Sandrock[23], J. Sandroos[39], M. Santander[54], S. Sarkar[44], S. Sarkar[25], K. Satalecka[59], M. Scharf[1], M. Schaufel[1], H. Schieler[31], S. Schindler[26], P. Schlunder[23], T. Schmidt[19], A. Schneider[38], J. Schneider[26], F. G. Schröder[31, 42], L. Schumacher[27], G. Schwefer[1], S. Sclafani[45], D. Seckel[42], S. Seunarine[47], A. Sharma[57], S. Shefali[32], M. Silva[38], B. Skrzypek[14], B. Smithers[4], R. Snihur[38], J. Soedingrekso[23], D. Soldin[42], C. Spannfellner[27], G. M. Spiczak[47], C. Spiering[59, 61], J. Stachurska[59], M. Stamatikos[21], T. Stanev[42], R. Stein[59], J. Stettner[1], A. Steuer[39], T. Stezelberger[9], T. Stürwald[58], T. Stuttard[22], G. W. Sullivan[19], I. Taboada[6], F. Tenholt[11], S. Ter-Antonyan[7], S. Tilav[42], F. Tischbein[1], K. Tollefson[24], L. Tomankova[11], C. Tönnis[53], S. Toscano[12], D. Tosi[38], A. Trettin[59], M. Tselengidou[26], C. F. Tung[6], A. Turcati[27], R. Turcotte[31], C. F. Turley[56], J. P. Twagirayezu[24], B. Ty[38], M. A. Unland Elorrieta[41], N. Valtonen-Mattila[57], J. Vandenbroucke[38], N. van Eijndhoven[13], D. Vannerom[15], J. van Santen[59], S. Verpoest[29], M. Vraeghe[29], C. Walck[50], T. B. Watson[4], C. Weaver[24], P. Weigel[15], A. Weindl[31], M. J. Weiss[56], J. Weldert[39], C. Wendt[38], J. Werthebach[23], M. Weyrauch[32], N. Whitehorn[24, 35], C. H. Wiebusch[1], D. R. Williams[54], M. Wolf[27], K. Woschnagg[8], G. Wrede[26], J. Wulff[11], X. W. Xu[7], Y. Xu[51], J. P. Yanez[25], S. Yoshida[16], S. Yu[24], T. Yuan[38], Z. Zhang[51]

[1] III. Physikalisches Institut, RWTH Aachen University, D-52056 Aachen, Germany
[2] Department of Physics, University of Adelaide, Adelaide, 5005, Australia
[3] Dept. of Physics and Astronomy, University of Alaska Anchorage, 3211 Providence Dr., Anchorage, AK 99508, USA
[4] Dept. of Physics, University of Texas at Arlington, 502 Yates St., Science Hall Rm 108, Box 19059, Arlington, TX 76019, USA
[5] CTSPS, Clark-Atlanta University, Atlanta, GA 30314, USA
[6] School of Physics and Center for Relativistic Astrophysics, Georgia Institute of Technology, Atlanta, GA 30332, USA
[7] Dept. of Physics, Southern University, Baton Rouge, LA 70813, USA
[8] Dept. of Physics, University of California, Berkeley, CA 94720, USA
[9] Lawrence Berkeley National Laboratory, Berkeley, CA 94720, USA
[10] Institut für Physik, Humboldt-Universität zu Berlin, D-12489 Berlin, Germany
[11] Fakultät für Physik & Astronomie, Ruhr-Universität Bochum, D-44780 Bochum, Germany
[12] Université Libre de Bruxelles, Science Faculty CP230, B-1050 Brussels, Belgium
[13] Vrije Universiteit Brussel (VUB), Dienst ELEM, B-1050 Brussels, Belgium
[14] Department of Physics and Laboratory for Particle Physics and Cosmology, Harvard University, Cambridge, MA 02138, USA
[15] Dept. of Physics, Massachusetts Institute of Technology, Cambridge, MA 02139, USA

[16] Dept. of Physics and Institute for Global Prominent Research, Chiba University, Chiba 263-8522, Japan

[17] Department of Physics, Loyola University Chicago, Chicago, IL 60660, USA

[18] Dept. of Physics and Astronomy, University of Canterbury, Private Bag 4800, Christchurch, New Zealand

[19] Dept. of Physics, University of Maryland, College Park, MD 20742, USA

[20] Dept. of Astronomy, Ohio State University, Columbus, OH 43210, USA

[21] Dept. of Physics and Center for Cosmology and Astro-Particle Physics, Ohio State University, Columbus, OH 43210, USA

[22] Niels Bohr Institute, University of Copenhagen, DK-2100 Copenhagen, Denmark

[23] Dept. of Physics, TU Dortmund University, D-44221 Dortmund, Germany

[24] Dept. of Physics and Astronomy, Michigan State University, East Lansing, MI 48824, USA

[25] Dept. of Physics, University of Alberta, Edmonton, Alberta, Canada T6G 2E1

[26] Erlangen Centre for Astroparticle Physics, Friedrich-Alexander-Universität Erlangen-Nürnberg, D-91058 Erlangen, Germany

[27] Physik-department, Technische Universität München, D-85748 Garching, Germany

[28] Département de physique nucléaire et corpusculaire, Université de Genève, CH-1211 Genève, Switzerland

[29] Dept. of Physics and Astronomy, University of Gent, B-9000 Gent, Belgium

[30] Dept. of Physics and Astronomy, University of California, Irvine, CA 92697, USA

[31] Karlsruhe Institute of Technology, Institute for Astroparticle Physics, D-76021 Karlsruhe, Germany

[32] Karlsruhe Institute of Technology, Institute of Experimental Particle Physics, D-76021 Karlsruhe, Germany

[33] Dept. of Physics, Engineering Physics, and Astronomy, Queen's University, Kingston, ON K7L 3N6, Canada

[34] Dept. of Physics and Astronomy, University of Kansas, Lawrence, KS 66045, USA

[35] Department of Physics and Astronomy, UCLA, Los Angeles, CA 90095, USA

[36] Department of Physics, Mercer University, Macon, GA 31207-0001, USA

[37] Dept. of Astronomy, University of Wisconsin–Madison, Madison, WI 53706, USA

[38] Dept. of Physics and Wisconsin IceCube Particle Astrophysics Center, University of Wisconsin–Madison, Madison, WI 53706, USA

[39] Institute of Physics, University of Mainz, Staudinger Weg 7, D-55099 Mainz, Germany

[40] Department of Physics, Marquette University, Milwaukee, WI, 53201, USA

[41] Institut für Kernphysik, Westfälische Wilhelms-Universität Münster, D-48149 Münster, Germany

[42] Bartol Research Institute and Dept. of Physics and Astronomy, University of Delaware, Newark, DE 19716, USA

[43] Dept. of Physics, Yale University, New Haven, CT 06520, USA

[44] Dept. of Physics, University of Oxford, Parks Road, Oxford OX1 3PU, UK

[45] Dept. of Physics, Drexel University, 3141 Chestnut Street, Philadelphia, PA 19104, USA

[46] Physics Department, South Dakota School of Mines and Technology, Rapid City, SD 57701, USA

[47] Dept. of Physics, University of Wisconsin, River Falls, WI 54022, USA

[48] Dept. of Physics and Astronomy, University of Rochester, Rochester, NY 14627, USA

[49] Department of Physics and Astronomy, University of Utah, Salt Lake City, UT 84112, USA

[50] Oskar Klein Centre and Dept. of Physics, Stockholm University, SE-10691 Stockholm, Sweden

[51] Dept. of Physics and Astronomy, Stony Brook University, Stony Brook, NY 11794-3800, USA

[52] Dept. of Physics, Sungkyunkwan University, Suwon 16419, Korea

[53] Institute of Basic Science, Sungkyunkwan University, Suwon 16419, Korea

[54] Dept. of Physics and Astronomy, University of Alabama, Tuscaloosa, AL 35487, USA

[55] Dept. of Astronomy and Astrophysics, Pennsylvania State University, University Park, PA 16802, USA

[56] Dept. of Physics, Pennsylvania State University, University Park, PA 16802, USA

[57] Dept. of Physics and Astronomy, Uppsala University, Box 516, S-75120 Uppsala, Sweden

[58] Dept. of Physics, University of Wuppertal, D-42119 Wuppertal, Germany

[59] DESY, D-15738 Zeuthen, Germany

[60] Università di Padova, I-35131 Padova, Italy

[61] National Research Nuclear University, Moscow Engineering Physics Institute (MEPhI), Moscow 115409, Russia

[62] Earthquake Research Institute, University of Tokyo, Bunkyo, Tokyo 113-0032, Japan

Acknowledgements

PoS(ICRC2021)1129